Supporting Information

Zaks et al. 10.1073/pnas.1211017109

SI Text

Model Structure. MATLAB code containing the equations used in the simulations can be found at the URL http://www.cchem.berkeley.edu/grfgrp/jzaks/supp/html/index.html. Overall, the structure of the model has the following form:

$$\dot{\boldsymbol{X}} = BG(I(t);p) + \sum_{k=1}^{8} A_k^T F_k(A_k \boldsymbol{X}, u_k; p) \qquad u_k = C_k \boldsymbol{X}. \quad \textbf{[S1]}$$

The variables in the model are vertically concatenated in vector $\boldsymbol{X}$. Each F_k consists of a module, as defined in the main text, that propagates some subset of the variables in vector $\boldsymbol{X}$. $G(I(t);p)$ is a scalar function relating the input (light intensity) to the evolution of light harvesting variables, and B is a 2×1 matrix relating the inputs to components of vector $\boldsymbol{X}$ that represent light harvesting chlorophylls in Photosystem II (PSII) and Photosystem I (PSI), contained in the functions F_1 and F_5. $G(I;p)$ does not depend on any components of $\boldsymbol{X}$, which means that the model assumes that the rate of light absorption by antenna chlorophylls is independent of the state of the photosynthetic apparatus. This assumption may need to be relaxed in the future if processes such as state transitions, which remove light harvesting complexes from PSII, are incorporated. The qE component of the model comprises a feedback loop because the input to qE is the lumen pH and qE itself is an input to the light harvesting module. A summary of the modules in the model is given in Table S1.

Because many variables are shared between modules, the differential equation at each time step for a given variable is determined by adding the contributions of differential equations from each module that affects that variable. For example, the number of protons in the lumen is affected by three modules: PSII, cytochrome b_6f, and ATP synthase; the resulting time-evolution of protons in the lumen is the sum of the contributions from these three modules.

Formally, to keep track of the distribution of variables into modules, we introduce the matrix A_k for each module k. A_k is a $m \times n$ matrix, where n is the length of $\boldsymbol{X}$ and m is the number of variables that are propagated by the function F_k. The matrix A_k has a 1 in each of its m rows to select the components of $\boldsymbol{X}$ that are propagated in module F_k. To sum the contributions from individual modules, each differential value $\dot{X}_k = F_k(X_k)$ is multiplied by the transpose of A_k. In the current implementation of the model, these matrices are generated automatically during the initiation phase (see file `initChloroplastSim` and `getIndices`)

Each module may require inputs of system variables in addition to those that that are propagated by that module. For example, qE quenching is activated by lumen pH but does not itself affect the pH, so the pH is an input to the module (F_2) for qE rather than a variable that is propagated by that module. Each module accepts an additional vector u_k that contains inputs for function $F_n(X_n)$. To calculate u_k at each time point in the simulation, the vector of variables X is multiplied by a matrix C_k of size $p \times n$, where p is the number of inputs to module k and n is, as before, the length of variable X.

Running the simulation. To run a simulation, the model requires (1) an sequence of light intensities and durations of these light intensities, (2) a vector of initial conditions, and (3) a set of values to use for each parameter. The time-step taken by the differential equation solver is determined by the differential equation solver provided in MATLAB (we use *ode15s*, but any stiff solver would in principle work). The solver varies the time-step of the simulation to balance efficiency of simulation with accuracy (1).

Units used in simulation. The variables for describing light-harvesting, qE quenching and electron transfer through the PSII reaction center and plastoquinone pool are expressed in terms of concentrations of number of molecules per PSII. To calculate the lumen pH and the proton motive force, we converted from number of molecules per PSII to molar concentrations.

Description of Modules. ***Energy transfer within PSII.*** Excited chlorophylls are quenched by energy transfer to the RC, by intrinsic decay processes, and by regulated NPQ pathways, as illustrated in Fig. 2*B* of the main text. Our model assumes a "lake" model of energy transfer in which quenching sites are shared between all excited chlorophylls (2), and that excitation equilibrates within PSII instantaneously before any photochemical or nonphotochemical quenching processes can take place. This assumption is a simplification because the timescale of energy transfer through the PSII antenna (3), as well as the exact location of the quenching site, will affect the relative yields of light harvesting and quenching energy. Nonetheless, because neither the exact nature of energy transfer through the PSII antenna (4) nor the exact site of qE quenching (5) are definitively known, our assumption is a necessary initial assumption and provides a framework for testing different models of energy transfer.

Electron transfer chain after PSII. For modeling energy transfer through PSII, electron transfer in the reaction center and through the plastoquinone pool, and plastoquinone reoxidation at cytochrome b_6f, we have followed previous models (6, 7). One notable modification is that we assumed that undocking of reduced plastoquinol and the docking of oxidized plastoquinol into the Q_B binding site had reverse rates that occurred at 10% of the rate of the forward reaction. We did this to improve agreement between simulated and measured Q_A oxidation state, typically measured as $1 - qP$ (2), at a range of light intensities, although accurate simulation of the oxidation state of Q_A at a range of light intensities requires further work. Following ref. (8), we assumed that the rate of plastoquinol oxidation at cytochrome b_6f slowed down at lower pH values, with a pK_a of 5.8 and Hill coefficient of 1.2, causing plastoquinol oxidation to be slower at lower pH. The pK_a value we used (5.8) is lower than the pKa value used in Takizawa et al. (6.6), but is closer to earlier estimates of the pH-dependence of plastoquinol oxidation (7). After passing through cytochrome b_6f, electrons are transferred to plastocyanin, then undergo another photoinduced electron transfer through the PSI reaction center, and finally to ferredoxin. Because calculating the redox state of the stroma (9) is beyond the scope of our current model, we assume that ferredoxin is rapidly reoxidized with a single rate constant.

Lumenal buffering and ion motion. To simulate the lumen pH, which triggers qE, it was necessary to calculate the rate of protons entering the lumen, the rate of protons leaving the lumen, and the buffering of protons inside the lumen. Protons enter the lumen at two points during linear electron flow: (1) water splitting at PSII and (2) plastoquinol oxidation at the cytochrome b_6f complex. Protons leave the lumen through ATP synthase, which converts the energy contained in the proton gradient across the thylakoid membrane to a phosphate bond in the molecule ATP. Overall,

under conditions of linear electron flow, three protons enter the lumen for each electron transferred through the PSII reaction center (10). These protons contribute to the proton motive force (*pmf*) in two ways (7): (1) by creating an electrical potential that drives positive charges to the outside of the lumen and (2) by creating a pH gradient that provides a diffusive potential for protons to exit the lumen. This parsing of the *pmf* into an electric field and a diffusion potential depends on the buffering capacity of the lumen and on the motion of charged ions across the thylakoid membrane (7).

The buffering of protons in the lumen has been studied in great detail in isolated chloroplasts (11) and a detailed mathematical model for lumenal buffering has also been developed (12), which indicates that the lumenal buffering capacity increases at decreasing pH. For simplicity, we use a constant buffering capacity of 30 mM protons per Δ pH (7). Nonetheless, incorporating a more accurate model of lumen buffering may be important in the future to achieve good agreement with a wider set of data, especially as the model is extended to incorporate plants in stressed conditions in which the lumen pH may be lowered past that of healthy plants.

The relationship between protons entering the lumen and the lumen pH also depends on the motion of ions in and out of the lumen. We have assumed that a significant portion of the proton motive force that drives ATP synthase is stored in the form of an electric field gradient across the thylakoid membrane, which occurs when the ionic strength of the lumen is low (5 mM) (7). In the absence of a *pmf* or electric field, which is what we assume the state of the system to be in the dark, the ion concentration of stroma and lumen are in equilibrium. In the light, the electric field formed by proton pumping exerts a driving force on the mobile ions within the lumen, which dissipate this electric field over time (7). Consequently, the fraction of the *pmf* that is stored as an electric field decreases over time as ions move across the thylakoid membrane and dissipate this electric field. This dissipation of the electric field increases the relative fraction of the *pmf* that must be stored as a Δ pH between lumen and stroma, and therefore lowers the lumen pH. The equations describing this process are taken from ref. (7). We use a concentration of 10 mM for the initial concentration of lumenal and stromal ion concentrations and assume that the stromal ion concentration does not change.

We assume that the volume of lumen per PSII is 6.7×10^{-21} L and that the ratio of lumen volume to surface area of the thylakoid membrane is 8×10^{-10} L/cm^2 (7). Because we have assumed that the proton motive force (*pmf*), which drives ATP synthesis, arises from both an electric field gradient ($\Delta\psi$) and Δ pH component, our model is consistent with recent views that sufficient *pmf* for ATP synthesis and qE can be attained at a moderate lumen pH (13).

Activation of ATP synthase. Accurately modeling the conductivity of ATP synthase is challenging because there are numerous factors regulating ATP synthesis (14). One possible approach is to assume, as in reference (7), that the ATP synthase has a constant proton conductivity. The problem with such an approach is that it does not incorporate the effect of the activation of the Calvin-Benson cycle by linear electron flow through the thioredoxin system (15), and as a result will overestimate the lumen pH in the initial few minutes when plants are moved from dark to light, especially in situations when the actinic light intensity does not saturate linear electron flow. At low light intensities, a transient qE appears within tens of seconds after the onset of illumination and disappears after several minutes, most likely because the ATP synthase enzyme is initially inactive, and its activity is activated along with the ATP-consuming reactions of the Calvin-Benson cycle (15).

To account for this transient qE without building a complex model of ATP synthase activation and ATP consumption, we have chosen to modulate the proton conductivity of ATP synthase with an effective average of the many processes that affect the rate of proton flux through ATP synthase. To model the rate of protons leaving the lumen through ATP synthase, we use the equation

$$H_{\text{out}} = g_{H^+} \times pmf \times F_{\text{ATP}}, \qquad \textbf{[S2]}$$

where g_{H^+} is the conductivity of ATP synthase, for which we use a value of 10^{-9} mol protons/V/cm^2/s, *pmf* is the proton motive force, and F_{ATP} is a unitless number between 0 and 1 that modulates the conductivity of ATP synthase. F_{ATP} increases with linear electron flow, and the rate of increase of F_{ATP} is a single rate representing all reactions that affect the rate of proton flux through ATP synthase. In the model F_{ATP} evolves according to the equation

$$\frac{dF_{\text{ATP}}}{dt} = k_{\text{ATPAct}}[Fdxr](1 - F_{\text{ATP}}) - k_{\text{ATPInact}}F_{\text{ATP}},$$

where $[Fdxr]$ is the fraction of the total ferredoxin in the stroma that is reduced. In fact, the factors controlling the rate of proton flux through ATP synthase are numerous and not fully understood, and include the activation of ATP synthase itself as well as the activation of several enzymes in the Calvin-Benson cycle that affect the consumption of ATP (16). Because the detailed dynamics of the carbon reactions and ATP synthase regulation are outside the scope of our model, we have chosen to capture the effect of the changing proton conductivity of ATP synthase during acclimation from dark-adapted to light-adapted state with a single rate constant, k_{ATPAct} and a reverse rate of inactivation, k_{ATPInact}. We note that this simplification reduces the applicability of our model to situations in which plants are stressed by, for example, cold or drought, though qE does play an important photoprotective role in these situations (17). More work is needed in order to be able to apply this model to such situations, where there may be significant potential for improving photosynthetic yields.

Proton to ATP ratio and cyclic electron flow. Cyclic electron flow (CEF) around PSI is an important process that affects qE in *Arabidopsis* (18). However, details of the regulation of CEF are not fully understood and are an area of current investigation (19). As a result, we have chosen to omit this process from our model and to compensate for its absence by altering the proton-to-ATP ratio of ATP synthase. Experimental and theoretical work has suggested that a major role of CEF is to set the ratio of ATP to NADPH production to be equal to 3:2, which is the ratio needed for the carbon reactions (20). It is thought that 14 protons are translocated through ATP synthase to form three molecules of ATP, causing the ratio of ATP to NADPH production to be lower than the 3:2 ratio needed for carbon reactions. If, instead, the ratio of protons to ATP produced by ATP synthase were 12:3, then ATP and NADPH production would be balanced with the demands of the Calvin-Benson cycle (20). If the role of CEF is indeed to balance the ratio of ATP and NADPH production with the ratio for their consumption, then assuming a proton to ATP ratio of 12:3 should lead to a more accurate estimate of lumen pH than if the effect of CEF were ignored completely. In our modeling, we have assumed that the proton-to-ATP ratio of ATP synthase enzyme is 12:3, which gives a 3:2 ratio of ATP to NADPH production.

Comparison Between Measured and Simulated PAM Fluorescence.

Extracting NPQ from PAM measurement. In a PAM fluorescence measurement, the data have been normalized to the initial dark-adapted fluorescence state F_o (21). While the plant is in the dark, an intense pulse of light measures the fluorescence yield of the plant when all PSII reaction centers are saturated, determining

the level of fluorescence (denoted F_m) before NPQ pathways have turned on. Upon transition from darkness to light, the fluorescence yield of the leaf rapidly increases to a maximal level, then decreases more slowly as the availability of photochemical and NPQ pathways increases. During repeated application of intense pulses (spikes) all reaction centers are fully closed, so the change in fluorescence quantum yield relative to F_m in the presence of these intense flashes (denoted F_m') is due to the appearance of NPQ pathways. A commonly used expression for total NPQ, which we also use, is NPQ $= (F_m - F_m')/F_m'$ (21, 22).

PAM simulation. The simulated qE curves shown in Fig. 4 of the main text were obtained from simulations of chlorophyll fluorescence as in the PAM fluorescence experiment (23). Fig. S1 shows the measurements (*Left*, *A* and *C*) and simulations (*Right*, *B* and *D*) of PAM fluorescence traces of dark adapted plants exposed to 100 μ mol photons m^{-2} s^{-1} (*Top*, *A*, *B*) and 1,000 μ mol photons m^{-2} s^{-1} (*Bottom*, *C*, *D*). Although Fig. 4 (main text) shows reasonable agreement between the model and data for qE, the deviation between the model and the full chlorophyll fluorescence trace is much greater. Because the model does not currently incorporate NPQ mechanisms other than qE, the height of the saturating spikes is constant in the simulation of the *npq4* mutant as shown in Fig. S1 *B* and *D*, in stark contrast to the measured data (Fig. S1 *B* and *D*). In particular, the model does not accurately calculate the baseline fluorescence level, denoted F_s, which is a measure of both photochemical and nonphotochemical quenching (21). The model calculates that photochemistry is fully saturated at 1,000 μ mol photons m^{-2} s^{-1}, leading to a completely flat and saturating fluorescence level in Fig. S1*D*. Because of the model's limitations in accurately calculating photochemical quenching, there is some discrepancy between experiment and model in the height of the spikes due to saturating pulses, which is used experimentally to measure the fraction of open reaction centers. However, we note that the trend of increasing height of the spikes as the plant adapts to light, which signifies a reduction in excitation pressure, is reproduced by the modeled activation of ATP synthase by linear electron flow.

Because the chlorophyll fluorescence is simulated according to Eq. **7** of the main text, the simulated rate of photochemical quenching is determined by the concentration of oxidized Q_A, independently of the redox state of Q_B or the PQ pool. In the model we used for electron transfer among quinones (6), the rate of electron transfer from Q_A to Q_B is much faster than the rate of downstream electron transfer reactions, and does not directly depend on the redox state of the PQ pool. Because of this, the transition from Q_A being fully reduced to fully oxidized in the model is much more abrupt than in reality. It is possible that the reason for these discrepancies is due to the fact that the model neglects processes other than electron transfer through PSII that may reduce the PQ pool, such as chlororespiration (24) and cyclic electron flow around PSI. In order to apply this model to incorporate the role of qE at a range of light intensities beyond the two example light intensities presented here, it will be necessary to refine the present model to correctly simulate the photochemistry that determines the dependence of the Q_A redox state on incident light intensity.

Model Parameters and Effect of Parameter Variation. Table S2 shows the numerical values of parameters affecting qE that were used to generate the simulations in Figs. 4–6 of the main text and Figs. S1–S4. Many of these values were fitted to achieve good agreement between experiment and data. The pKa and Hill coefficient of PsbS protonation that we used are 6.3 and 3, respectively, which are somewhat different from the values of 6.8 and 1 found by Takizawa et al. (8). This discrepancy is probably due to the fact that, in Takizawa et al., in vivo estimates of lumen pH derived from measurements of the electrochromic shift were used to fit to steady state NPQ values for various mutants; in this work, we fit NPQ of only the wild type to dynamic NPQ measurements.

To assess the effect of varying parameters on the conclusion of Fig. 6 in the main text, which is that qE does not change the lumen pH, we plotted the lumen pH in the presence and absence of qE for a range of ATP synthase conductivities and rate of ATP synthase activation in Fig. S3. For all these parameter values, the lumen pH was not affected by qE. Varying the conductivity of ATP synthase did affect the redox state of Q_A (Fig. S4*A*) and of the plastoquinone pool (Fig S4*B*). The fact that the lumen pH appears to be unchanged is likely due to the fact that the rate limiting step for linear electron flow occurs at the cytochrome b_6f complex (25).

1. Shampine LF, Reichelt MW (1997) The MATLAB ODE suite. *SIAM J Sci Comput* 18:1–22.
2. Kramer D, Johnson G, Kiirats O, Edwards G (2004) New fluorescence parameters for the determination of Q_A redox state and excitation energy fluxes. *Photosynth Res* 79:209–218.
3. van Oort B, et al. (2010) Effect of antenna-depletion in Photosystem II on excitation energy transfer in *Arabidopsis thaliana*. *Biophys J* 98:922–931.
4. Renger T, Schlodder E (2010) Primary photophysical processes in Photosystem II: Bridging the gap between crystal structure and optical spectra. *Chem Phys Chem* 11:1141–1153.
5. Ruban AV, Johnson MP, Duffy CDP (2012) The photoprotective molecular switch in the photosystem II antenna. *Biochim Bhiophys Acta* 1817:167–181.
6. Belyaeva NE, et al. (2008) PS II model-based simulations of single turnover flash-induced transients of fluorescence yield monitored within the time domain of 100 ns–10 s on dark-adapted *Chlorella pyrenoidosa* cells. *Photosynth Res* 98:105–119.
7. Cruz JA, Sacksteder CA, Kanazawa A, Kramer DM (2001) Contribution of electric field (Δ psi) to steady-state transthylakoid proton motive force (*pmf*) in vitro and in vivo. control of pmf parsing into Delta psi and Delta pH by ionic strength. *Biochemistry* 40:1226–1237.
8. Takizawa K, Cruz JA, Kanazawa A, Kramer DM (2007) The thylakoid proton motive force in vivo. Quantitative, non-invasive probes, energetics, and regulatory consequences of light-induced pmf. *Biochim Bhiophys Acta* 1767:1233–1244.
9. Scheibe R (2005) Strategies to maintain redox homeostasis during photosynthesis under changing conditions. *J Exp Bot* 56:1481–1489.
10. Sacksteder CA, Kanazawa A, Jacoby ME, Kramer DM (2000) The proton to electron stoichiometry of steady-state photosynthesis in living plants: A proton-pumping Q cycle is continuously engaged. *Proc Natl Acad Sci USA* 97:14283–14288.
11. Junge W, McLaughlin S (1987) The role of fixed and mobile buffers in the kinetics of proton movement. *Biochim Bhiophys Acta* 890:1–5.
12. van Kooten O, Snel J, Vredenberg WJ (1986) Photosynthetic free energy transduction related to the electric potential changes across the thylakoid membrane. *Photosynth Res* 9:211–227.
13. Kramer DM, Sacksteder CA, Cruz JA (1999) How acidic is the lumen? *Photosynth Res* 60:151–163.
14. Kanazawa A, Kramer DM (2002) In vivo modulation of nonphotochemical exciton quenching (NPQ) by regulation of the chloroplast ATP synthase. *Proc Natl Acad Sci USA* 99:12789–12794.
15. Kalituho L, Beran KC, Jahns P (2007) The transiently generated nonphotochemical quenching of excitation energy in Arabidopsis leaves is modulated by zeaxanthin. *Plant Physiol* 143:1861–1870.
16. Buchanan BB (1980) Role of light in the regulation of chloroplast enzymes. *Annu Rev Plant Physiol* 31:341–374.
17. Bravo LA, et al. (2007) Effect of cold acclimation on the photosynthetic performance of two ecotypes of Colobanthus quitensis (Kunth) Bartl. *J Exp Bot* 58:3581–3590.
18. Munekage Y, et al. (2004) Cyclic electron flow around photosystem I is essential for photosynthesis. *Nature* 429:579–582.
19. Livingston AK, Kanazawa A, Cruz JA, Kramer DM (2010) Regulation of cyclic electron flow in C3 plants: Differential effects of limiting photosynthesis at ribulose-1,5-bisphosphate carboxylase/oxygenase and glyceraldehyde-3-phosphate dehydrogenase. *Plant Cell Environ* 33:1779–1788.
20. Kramer DM, Avenson TJ, Edwards GE (2004) Dynamic flexibility in the light reactions of photosynthesis governed by both electron and proton transfer reactions. *Trends Plant Sci* 9:349–357.
21. Baker NR (2008) Chlorophyll fluorescence: A probe of photosynthesis in vivo. *Annu Rev Plant Biol* 61:89–113.
22. Ahn TK, et al. (2009) Investigating energy partitioning during photosynthesis using an expanded quantum yield convention. *Chem Phys* 357:151–158.
23. Brooks MD, Niyogi KK (2011) in *Chloroplast Research in Arabidopsis: Methods and Protocols, Volume II*, ed Jarvis RP (Springer, Heidelberg), pp 299–310.
24. Field TS, Nedbal L, Ort DR (1998) Nonphotochemical reduction of the plastoquinone pool in sunflower leaves originates from chlororespiration. *Plant Physiol* 116:1209–1218.
25. Rochaix J-D (2011) Regulation of photosynthetic electron transport. *Biochim Bhiophys Acta* 1807:375–383.

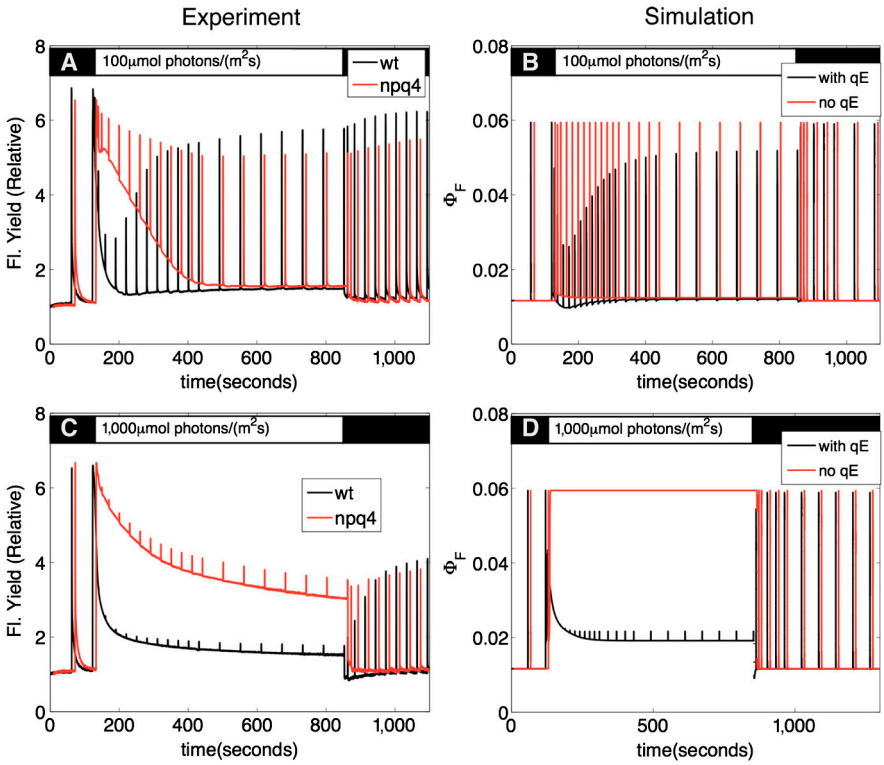

Fig. S1. Measured (*A*, *C*) and simulated (*B*, *D*) chlorophyll fluorescence yield of *Arabidopsis thaliana* leaves at different light intensities with (black) and without (red) qE. The discrepancy between the *npq4* experiment and the no qE simulation is large because our model does not incorporate slowly reversible components of nonphotochemical quenching. The black bar at the top indicates times when the leaf is in the dark, and the white bar indicates times when the leaf is illuminated by actinic light illumination.

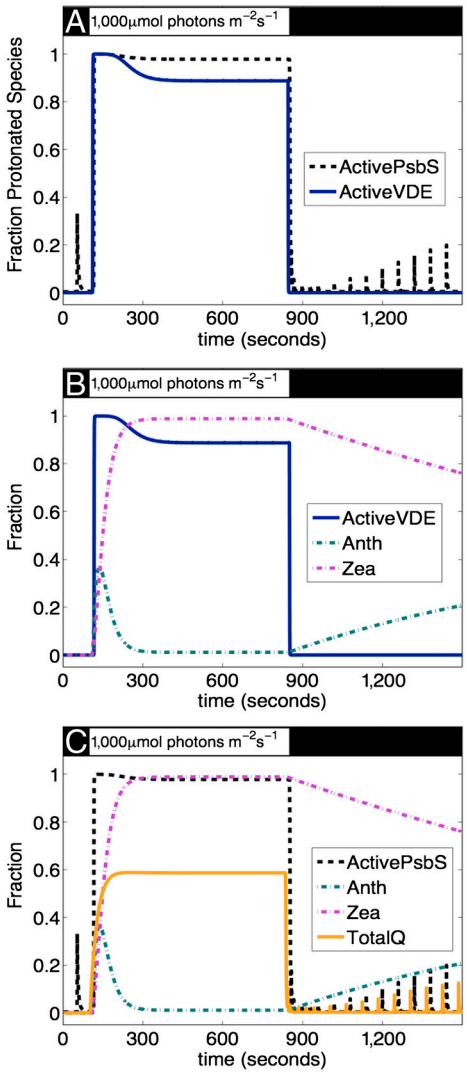

Fig. S2. Evolution of quenching species at 1,000 μmol photons/m^2/s. Simulations done with the same parameters as those used in Fig. 4*A* of the main text. Key parameters are given in Table S2. The black bar at the top indicates times when the plant is darkened, and the white bar indicates actinic light illumination. (*A*) Fraction of PsbS (black) and violaxanthin deepoxidase (blue) that are activated by the lumen pH. (*B*) Activity of violaxanthin deepoxidase (blue) and fraction of xanthophyll that is in the form of antheraxanthin (green) and zeaxanthin (red) in a qE-relevant binding site that is made from violaxanthin by VDE. (*C*) Fraction of total qE quenching sites with protonated PsbS (black), zeaxanthin or antheraxanthin (green/red) and active qE quenching pathways (orange), assuming Eq. **3** of the main text. The rate of qE induction is slower than the rate of qE relaxation because, in our model, qE induction is limited by VDE activity, whereas PsbS is deactivated rapidly, turning qE off.

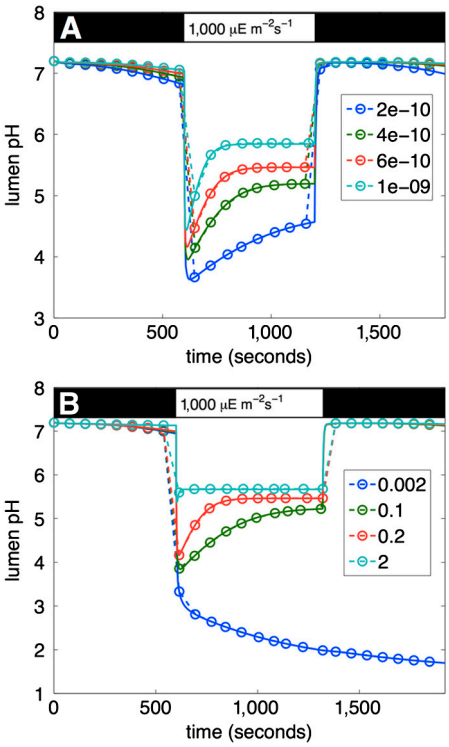

Fig. S3. Simulated lumen pH values with qE (circles with dashes) and without qE (lines) quenching for different values of (*A*) ATP conductivity, in units of mol protons/V/cm^2/s and (*B*) rate of activation of ATP synthase through ferredoxin, in units of active ATP synthase/PSII/second/reduced ferredoxin. The rate of ATP synthase deactivation was kept constant.

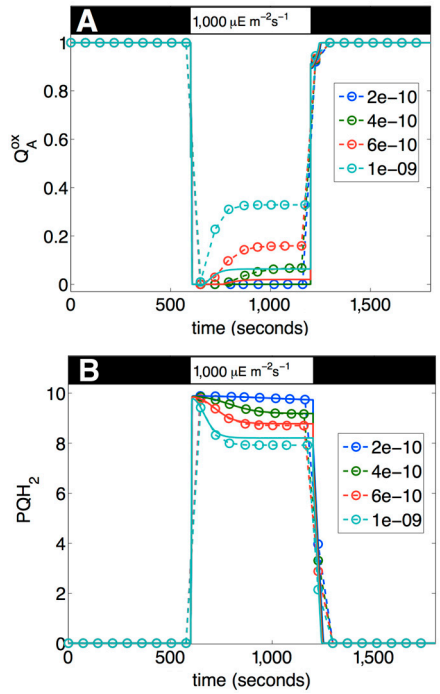

Fig. S4. Simulated (*A*) Oxidized Q_A and (*B*) Reduced plastoquinol (PQH_2) values with qE (circles with dashes) and without qE (lines) quenching for different values of ATP synthase conductivity, in units of mol protons/Volt/cm^2/s

Table S1. Model components and references

Module	References (if available)
(F_1) light harvesting	(1–4)
(F_2) qE quenching	(5, 6)
(F_3) electron transfer through plastoquinone pool	(1)
(F_4) plastoquinol oxidation at cytochrome b_6f	(5, 7)
(F_5) electron transfer through plastocyanin and PSI on to ferredoxin	(8)
(F_6) reduction of the stroma by ferredoxin	—
(F_7) activation of proton efflux via the ATP synthase enzyme	—
(F_8) proton and ion dynamics in the lumen and stroma	(7)

1 Belyaeva NE, et al. (2008) PS II model-based simulations of single turnover flash-induced transients of fluorescence yield monitored within the time domain of 100 ns–10 s on dark-adapted *Chlorella pyrenoidosa* cells. *Photosynth Res* 98:105–119.

2 Rubin A, Riznichenko G (2011) *Photosynthesis in Silico: Understanding Complexity from Molecules to Ecosystems*, eds Laisk A, Govindjee (2009 Springer, Heidelberg), pp 151–176.

3 Lebedeva GV, Belyaeva NE, Demin OV, Riznichenko GYu, Rubin AB (2002) Kinetic model of primary photosynthetic processes in chloroplasts. Description of the fast phase of chlorophyll fluorescence induction under different light intensities. *Biofizika* 47:1044–1058.

4 Zhu X-G, Ort DR, Whitmarsh J, Long, SP (2004) The slow reversibility of photosystem II thermal energy dissipation on transfer from high to low light may cause large losses in carbon gain by crop canopies: A theoretical analysis. *J Exp Bot* 55:1167–1175.

5 Takizawa K, Cruz JA, Kanazawa A, Kramer DM (2007) The thylakoid proton motive force in vivo. Quantitative, non-invasive probes, energetics, and regulatory consequences of light-induced pmf. *Biochim Bhiophys Acta* 1767:1233–1244.

6 Li X-P, Muller-Moule P, Gilmore AM, Niyogi KK (2002) PsbS-dependent enhancement of feedback de-excitation protects photosystem II from photoinhibition. *Proc Natl Acad Sci USA* 99:15222–15227.

7 Cruz JA, Sacksteder CA, Kanazawa A, Kramer DM (2001) Contribution of electric field (Δ psi) to steady-state transthylakoid proton motive force (*pmf*) in vitro and in vivo. control of pmf parsing into Delta psi and Delta pH by ionic strength. *Biochemistry* 40:1226–1237.

8 Sacksteder CA, Kanazawa A, Jacoby ME, Kramer DM (2000) The proton to electron stoichiometry of steady-state photosynthesis in living plants: A proton-pumping Q cycle is continuously engaged. *Proc Natl Acad Sci USA* 97:14283–14288.

Table S2. Values of parameters affecting qE used in simulations

Parameter	Value	Explanation and source
$k_{VDE,VA}$	4×10^{-2} s^{-1}	rate of deepoxidation from violaxanthin to antheraxanthin (1)
$k_{VDE,AZ}$	4×10^{-2} s^{-1}	rate of deepoxidation from antheraxanthin to zeaxanathin (fitted)
k_{ZE}	4×10^{-4} s^{-1}	rate of violaxanthin and antheraxanthin epoxidation (fitted)
pKa VDE	6.0	pKa of VDE activation (2, 3)
nVDE	6	Hill coefficient of VDE activation (fitted)
pKa of PsbS	6.4	pKa of PsbS activation (fitted)
nPsbS	3	Hill coefficient of PsbS activation (fitted)
PsbS Dose	0.6	Fraction of possible quenching sites that are triggered by PsbS (fitted)

1 Takizawa K, Cruz JA, Kanazawa A, Kramer DM (2007) The thylakoid proton motive force in vivo. Quantitative, non-invasive probes, energetics, and regulatory consequences of light-induced pmf. *Biochim Bhiophys Acta* 1767:1233–1244.

2 Kalituho L, Beran KC, Jahns P (2007) The transiently generated nonphotochemical quenching of excitation energy in Arabidopsis leaves is modulated by zeaxanthin. *Plan Physiol* 143:1861–1870.

3 Jahns P, Latowski D, Strzalka K (2009) Mechanism and regulation of the violaxanthin cycle: The role of antenna proteins and membrane lipid. *Biochim Bhiophys Acta* 1787:3–14.